

# New Test Beam Results of 3D and Pad Detectors Constructed with Poly-Crystalline CVD Diamond

M. Reichmann<sup>x,\*</sup>, A. Alexopoulos<sup>c</sup>, M. Artuso<sup>t</sup>, F. Bachmair<sup>x</sup>, L. Bäni<sup>x</sup>,  
M. Bartosik<sup>c</sup>, J. Beacham<sup>m</sup>, H. Beck<sup>w</sup>, V. Bellini<sup>b</sup>, V. Belyaev<sup>l</sup>, B. Bentele<sup>s</sup>,  
A. Bes<sup>aa</sup>, J.-M. Brom<sup>g</sup>, M. Bruzzi<sup>d</sup>, G. Chiodini<sup>z</sup>, D. Chren<sup>r</sup>, V. Cindro<sup>i</sup>,  
G. Claus<sup>g</sup>, J. Collot<sup>aa</sup>, J. Cumalat<sup>s</sup>, A. Dabrowski<sup>c</sup>, R. D'Alessandro<sup>d</sup>,  
D. Dauvergne<sup>aa</sup>, W. de Boer<sup>j</sup>, S. Dick<sup>m</sup>, C. Dorfer<sup>x</sup>, M. Dünser<sup>c</sup>, G. Eigen<sup>ad</sup>,  
V. Eremin<sup>f</sup>, G.T. Forcolin<sup>v</sup>, J. Forneris<sup>o</sup>, L. Gallin-Martel<sup>aa</sup>,  
M.L. Gallin-Martel<sup>aa</sup>, K.K. Gan<sup>m</sup>, M. Gastal<sup>c</sup>, C. Giroletti<sup>a</sup>, M. Goffe<sup>g</sup>,  
J. Goldstein<sup>q</sup>, A. Golubev<sup>h</sup>, A. Gorišek<sup>i</sup>, E. Grigoriev<sup>h</sup>, J. Grosse-Knetter<sup>w</sup>,  
A. Grummer<sup>u</sup>, B. Gui<sup>m</sup>, M. Guthoff<sup>c</sup>, B. Hiti<sup>i</sup>, D. Hits<sup>x</sup>, M. Hoferkamp<sup>u</sup>,  
T. Hofmann<sup>c</sup>, J. Hosselet<sup>g</sup>, J.-Y. Hostachy<sup>aa</sup>, F. Hügging<sup>a</sup>, C. Hutton<sup>q</sup>,  
J. Janssen<sup>a</sup>, H. Kagan<sup>m</sup>, K. Kanxheri<sup>ab</sup>, G. Kasieczka<sup>x</sup>, R. Kass<sup>m</sup>, M. Kis<sup>e</sup>,  
G. Kramberger<sup>i</sup>, S. Kuleshov<sup>h</sup>, A. Lacoste<sup>aa</sup>, S. Lagomarsino<sup>d</sup>, A. Lo Giudice<sup>o</sup>,  
I. López Paz<sup>v</sup>, E. Lukosi<sup>y</sup>, C. Maazouzi<sup>g</sup>, I. Mandic<sup>i</sup>, A. Marino<sup>s</sup>, C. Mathieu<sup>g</sup>,  
M. Menichelli<sup>ab</sup>, M. Mikuz<sup>i</sup>, A. Morozzi<sup>ab</sup>, J. Moss<sup>ac</sup>, R. Mountain<sup>t</sup>, A. Oh<sup>v</sup>,  
P. Olivero<sup>o</sup>, D. Passeri<sup>ab</sup>, H. Pernegger<sup>c</sup>, R. Perrino<sup>z</sup>, M. Piccini<sup>ab</sup>, F. Picollo<sup>o</sup>,  
M. Pomorski<sup>k</sup>, R. Potenza<sup>b</sup>, A. Quadt<sup>w</sup>, F. Rarbi<sup>aa</sup>, A. Re<sup>o</sup>, S. Roe<sup>c</sup>,  
D.A. Sanz Becerra<sup>x</sup>, M. Scaringella<sup>d</sup>, C.J. Schmidt<sup>e</sup>, E. Schioppa<sup>c</sup>,  
S. Schnetzer<sup>n</sup>, S. Sciortino<sup>d</sup>, A. Scorzoni<sup>ab</sup>, S. Seidel<sup>u</sup>, L. Servoli<sup>ab</sup>,  
D.S. Smith<sup>m</sup>, B. Sopko<sup>r</sup>, V. Sopko<sup>r</sup>, S. Spagnolo<sup>z</sup>, S. Spanier<sup>y</sup>, K. Stenson<sup>s</sup>,  
R. Stone<sup>n</sup>, B. Stugo<sup>ad</sup>, C. Sutura<sup>b</sup>, B. Tannenwald<sup>m</sup>, M. Traeger<sup>e</sup>,  
W. Trischuk<sup>p</sup>, D. Tromson<sup>k</sup>, M. Truccato<sup>o</sup>, C. Tuve<sup>b</sup>, J. Velthuis<sup>q</sup>,  
N. Venturi<sup>c</sup>, S. Wagner<sup>s</sup>, R. Wallny<sup>x</sup>, J.C. Wang<sup>t</sup>, J. Weingarten<sup>w</sup>, C. Weiss<sup>c</sup>,  
N. Wermes<sup>a</sup>, M. Yamouni<sup>aa</sup>, M. Zalieckas<sup>ad</sup>, M. Zavrtanik<sup>i</sup>, P.S. Salter<sup>ae</sup>,  
M. Chmeissani<sup>af</sup>, S. Grinstein<sup>af</sup>, D. Vazquez Furelos<sup>af</sup>

<sup>a</sup>Universität Bonn, Bonn, Germany, <sup>b</sup>INFN/University of Catania, Catania, Italy,  
<sup>c</sup>CERN, Geneva, Switzerland, <sup>d</sup>INFN/University of Florence, Florence, Italy, <sup>e</sup>GSI,  
Darmstadt, Germany, <sup>f</sup>Ioffe Institute, St. Petersburg, Russia, <sup>g</sup>IPHC, Strasbourg,  
France, <sup>h</sup>ITEP, Moscow, Russia, <sup>i</sup>Jožef Stefan Institute, Ljubljana, Slovenia,  
<sup>j</sup>Universität Karlsruhe, Karlsruhe, Germany, <sup>k</sup>CEA-LIST Technologies Avancees, Saclay,  
France, <sup>l</sup>MEPHI Institute, Moscow, Russia, <sup>m</sup>The Ohio State University, Columbus,  
OH, USA, <sup>n</sup>Rutgers University, Piscataway, NJ, USA, <sup>o</sup>University of Torino, Torino,  
Italy, <sup>p</sup>University of Toronto, Toronto, ON, Canada, <sup>q</sup>University of Bristol, Bristol, UK,  
<sup>r</sup>Czech Technical University, Prague, Czech Republic, <sup>s</sup>University of Colorado, Boulder,  
CO, USA, <sup>t</sup>Syracuse University, Syracuse, NY, USA, <sup>u</sup>University of New Mexico,  
Albuquerque, NM, USA, <sup>v</sup>University of Manchester, Manchester, UK, <sup>w</sup>Universität  
Göttingen, Göttingen, Germany, <sup>x</sup>ETH Zürich, Zürich, Switzerland, <sup>y</sup>University of  
Tennessee, Knoxville, TN, USA, <sup>z</sup>INFN-Lecce, Lecce, Italy, <sup>aa</sup>LPSC-Grenoble, Grenoble,  
France, <sup>ab</sup>INFN-Perugia, Perugia, Italy, <sup>ac</sup>California State University, Sacramento, CA,  
USA, <sup>ad</sup>University of Bergen, Bergen, Norway, <sup>ae</sup>University of Oxford, Oxford, UK,  
<sup>af</sup>Institut de Física d'Altes Energies (IFAE), ICREA and BIST, Barcelona, Spain,

---

\*Corresponding author

---

## Abstract

Chemical Vapour Deposition (CVD) diamond is being considered as a material for particle detectors in a harsh radiation environment. This article presents beam test results of 3D pixel detectors fabricated with poly-crystalline CVD diamonds. The cells of the devices had a size of  $50\text{ }\mu\text{m} \times 50\text{ }\mu\text{m}$  with columns  $2.6\text{ }\mu\text{m}$  in diameter. The cells were ganged in a  $3 \times 2$  and  $5 \times 1$  pattern to match the layouts of the pixel read-out electronics currently used in the CMS and ATLAS experiments at the Large Hadron Collider, respectively. In beam tests, using tracks reconstructed with a high precision tracking telescope, a tracking efficiency of 99.3% was achieved. The efficiency of both devices plateaus at a bias voltage of 30 V. Also irradiated poly-crystalline CVD diamond pad detectors were investigated. In high rate beam tests with particle fluxes up to  $20\text{ MHz/cm}^2$  and irradiations up to  $8 \cdot 10^{15}\text{ n/cm}^2$  it was shown that the pulse height of irradiated poly-crystalline CVD diamonds does not depend on flux to the  $\mathcal{O}(2\%)$ .

*Keywords:* Chemical Vapour Deposition, pCVD diamond, diamond detectors, 3D diamond detectors, 3D sensors, radiation tolerant detectors, particle flux

---

## 1. Introduction

The radiation levels of the High-Luminosity Large Hadron Collider (HL-LHC) are expected to be a big challenge for the future detectors. By 2028 experiments must be prepared for an instantaneous luminosity of  $7.5 \cdot 10^{34}\text{ cm}^{-2}\text{ s}^{-1}$ . In this  
5 environment the innermost tracking layer at a transverse distance of  $\sim 30\text{ mm}$  to the interaction point will be exposed to a total fluence of  $2 \cdot 10^{16}\text{ n}_{\text{eq}}/\text{cm}^2$  which corresponds to a total dose of the  $\mathcal{O}(10\text{ MGy})$  [1]. After such a large dose, all detector materials become trap limited with a schubweg below  $75\text{ }\mu\text{m}$ . The expected lifetime of the current planar silicon tracking detectors would be  
10 about one year in such and environment.

Due to the properties of CVD diamond, such as the displacement energy of 42 eV/atom and the band gap of 5.5 eV, the RD42 collaboration is investigating it as a possible detector material [2]. Compared to analogous silicon detectors, various studies have shown that diamond is at a minimum three times more  
15 radiation hard [3], collects the charges at least two times faster [4] and conducts heat four times more efficiently [5].

By now the technology of diamond detectors is well established in high energy physics. Many high energy physics experiments are already using Beam Condition Monitors or Beam Loss Monitors based on CVD diamonds [6, 7, 8].

20 The RD42 collaboration is studying a novel detector design in diamond, namely 3D detectors. The 3D concept reduces the drift distance an electron-hole pair must undergo to reach an electrode below the schubweg of an irradiated sensor without reducing the amount of created electron-hole pairs.

The particle flux of the HL-LHC will also reach a completely new regime.  
25 Hence it is important to study all proposed detectors at high rates of particles.

## 2. 3D Pixel Detectors

By placing column-like electrodes inside the detector material, the 3D geometry reduces the drift distance of a charge created by ionising particles compared to a planar device. More details about the working principle can be found in [9],  
30 [10]. All devices discussed in this article were constructed with poly-crystalline CVD (pCVD) diamond.

### 2.1. Fabrication

In order to manufacture the electrodes in diamond, columns were fabricated using a 130 fs laser with a wavelength of 800 nm which converts the diamond  
35 into a electrically resistive mixture of different carbon phases [11]. A Spatial Light Modulator (SLM) was used to correct aberrations during fabrication to achieve a column yield of >99 %, a column diameter of 2.6  $\mu\text{m}$  and a resistivity of the columns of the order of 0.1  $\sim$  1  $\Omega\text{ cm}$  [12]. The columns are not drilled

completely through the diamond, but with a gap of  $15\text{ }\mu\text{m}$  to the opposite surface  
 40 to avoid high voltage breakthrough. The largest fabricated device had about  
 4000 3D cells, where one cell consists of four bias electrodes and one readout  
 electrode in the centre.

The detector was constructed by connecting the bias columns with a metalli-  
 sation on the bottom surface and the readout columns with a metallisation on  
 45 the top surface and bump bonding the sensor to the readout electronics as shown  
 in Figure 1. For the detectors described herein a cell size of  $50\text{ }\mu\text{m} \times 50\text{ }\mu\text{m}$  was  
 chosen. Since the layout of the available readout chips (ROCs) has a different  
 pixel pitch several cells were ganged together. A photograph of an assembled

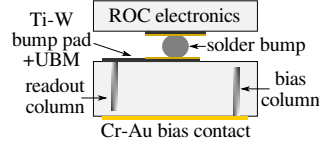


Figure 1: Bump bonding scheme.

3D detector on a ROC is shown in Figure 2.

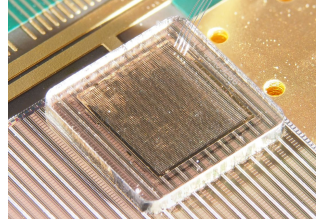


Figure 2: Final 3D pixel detector.

## 50 2.2. *PSI46digV2.1respin readout*

The first prototype of a  $50\text{ }\mu\text{m} \times 50\text{ }\mu\text{m}$  3D pixel detector was connected to  
 the PSI46digV2.1respin ROC [13] with a  $3 \times 2$  cell ganging to match the pixel  
 pitch of  $150\text{ }\mu\text{m} \times 100\text{ }\mu\text{m}$ . The 3D sensors were bump bonded to the ROC at  
 the Nanofabrication Lab at the Princeton University with indium bumps by

55 putting equal height indium columns on both ROC and the sensor and then pressing them together.

We define the hit efficiency as the percentage of hits in the 3D pixel detector when a particle track traversed the detector. The preliminary beam test results show that, relative to a planar silicon device, the efficiency in the fiducial area was 99.3% (Figure 3a). This efficiency estimation does not account for  
60 non-working 3D cells in this region which can happen due to broken or missing columns or due to metalisation issues. An area with a void in the diamond, where several columns could not be drilled, is highlighted below the fiducial area. In order to acquire this information further data will be analysed. Nevertheless, a small mismatch between a 3D and a planar device is expected due to  
65 a region inside the cells where the electric field is low [14] and due to the relative inefficiency of the columns themselves. Figure 3b shows that the device plateaus at a voltage of 30 V. The preliminary analysis of the pulse height distribution yields a mean value of  $\sim 11$  ke. The precise pulse height calibration of the ROC is currently being studied.



(a) Efficiency map. The red box marks the fiducial area. (b) Efficiency vs. voltage in the fiducial area.

Figure 3: Hit efficiency results with PSI46digV2.1respin readout.

70

### 2.3. FE-I4b readout

The second prototype was connected to the FE-I4b ROC [15] with a  $5 \times 1$  cell ganging due to the ROC pitch of  $250 \mu\text{m} \times 50 \mu\text{m}$ . The bump bonding was performed at IFAE-CNM in Barcelona by an adapted process with tin-

75 silver bumps. Using a high resolution beam telescope, with a spatial resolution of  $3\text{ }\mu\text{m}$  at the device under test, the efficiency could be mapped to the spatial coordinates. The analysis yields an efficiency of 97.8 % in the contiguous fiducial

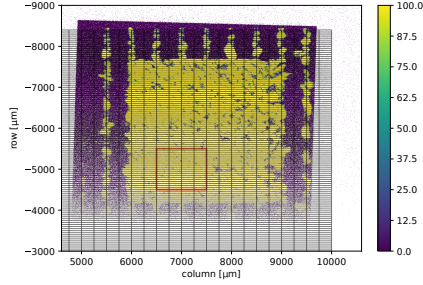


Figure 4: Hit efficiency results with the FE-I4b readout. The red box denotes the fiducial area.

area (Figure 4). The efficiency being lower than 99 % is most likely due to issues with the bump bonding or the metallisation as indicated by the inefficient patches in the efficiency map. The preliminary pulse height in the fiducial region was  $\sim 15\text{ ke}$  which is consistent with the result of the first prototype considering the different momenta of the incident particles (260 MeV/c for prototype 1 and 120 GeV/c for prototype 2). The precise pulse height calibration for the FE-I4b ROC is in the process of being performed.

### 85 3. High Rate Studies

At the HL-LHC particle fluxes will reach the  $\mathcal{O}(\text{GHz}/\text{cm}^2)$  hence it is very important to understand the effect of the incident particle flux on the signal of all prospective detectors. In order to conduct a high rate study it is necessary to be able to vary the particle flux over a large range. The  $\pi\text{M1}$  beam line at the High Intensity Proton Accelerator (HIPA) at Paul Scherrer Institut (PSI) [16] can provide beams with continuously tunable fluxes from the order of  $1\text{ kHz}/\text{cm}^2$  up to  $20\text{ MHz}/\text{cm}^2$ . The  $\pi\text{M1}$  beam is bunched with a spacing of  $19.7\text{ ns}$ . For these studies a  $\pi^+$  beam with a momentum of  $260\text{ MeV}/c$  was chosen in order to

reach the highest possible flux [17]. In total 13 pCVD diamonds were measured  
 95 which were all prepared in the same way.

### 3.1. Setup

The planar diamond sensors were connected in a pad geometry and prepared  
 as described in [18]. In order to resolve individual particles at high particle rates  
 the sensors were connected to a fast amplifier with low electronic noise and a  
 100 rise time of approximately 5 ns. The resulting waveforms were digitised and  
 recorded in a beam telescope setup [18] which provides spatial information of  
 the hits in the diamond detector. Due to the low momentum of the incident  
 particles the spatial resolution of the telescope was of the  $\mathcal{O}(100\mu\text{m})$ .

### 3.2. Results

105 In order to measure the signal behaviour as a function of incident particle  
 flux and irradiation, several rate scans with both polarities of the bias voltage

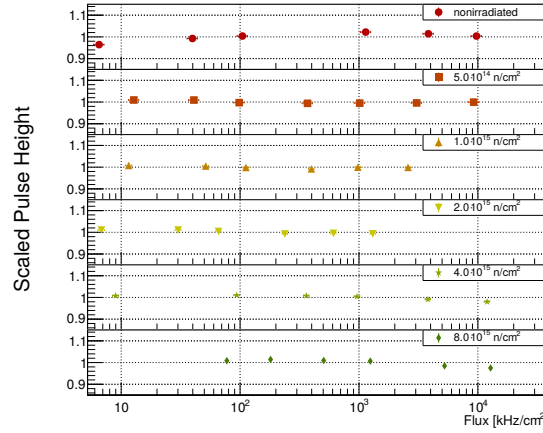


Figure 5: Pulse height versus incident particle flux for a pCVD diamond for various fluences  
 at a bias voltage of  $-1000\text{ V}$ .

were performed. Figure 5 shows the preliminary results for a pCVD diamond  
 with various fluences up to a maximum particle flux of  $20\text{ MHz/cm}^2$  at a bias  
 voltage of  $-1000\text{ V}$ . In order to compare several different irradiations the sensor  
 110 was irradiated with fast reactor neutrons in several steps up to total fluence of

$8 \cdot 10^{15} \text{ n/cm}^2$ . This was achieved at the irradiation facilities at the JSI TRIGA reactor in Ljubljana [19] prior to the beam tests at PSI. The mean pulse height of the single rate scans is scaled to 1. The results show that the pulse height is flat with respect to the flux deviating less than 2 % from the mean.

115 The effect of particle rate on the beam induced current in diamond detectors was also measured. 80 % of the measured diamonds had currents proportional to the flux and a leakage current without a beam of the  $\mathcal{O}(1 \text{ nA})$ . The other 20 % show shifting base lines or erratic dark currents [20]. These diamonds are considered problematic and were not analysed for this article.

120 pCVD diamond has an interior crystal structure where the individual grains have slightly different properties. Therefore the size of the measured signal in pCVD diamond can also depend on the spatial position as can be seen in Figure 6. A constant fiducial region was used to minimise any effects of the spatial dependence.

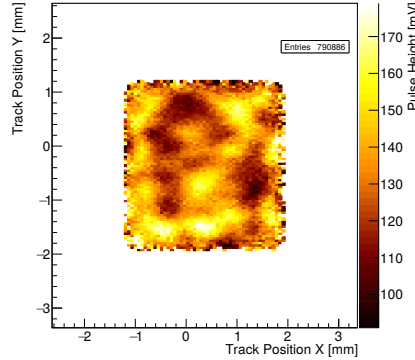


Figure 6: Pulse height map of a pCVD diamond as a function of spatial position.

125 We also observed a single diamond with a large rate dependence losing 90 % of the signal at the highest rate. After the surface was cleaned and processed with Reactive Ion Etching (RIE), the device was re-metallised. A new measurement showed a deviation of less than 2 % from the mean pulse height. This leads us to the conclusion that this rate effect was due to surface properties and  
130 is possible to repair.



#### 4. Conclusion

There is progress in the development of radiation tolerant particle detectors based on pCVD diamonds. The working principle of 3D diamond pixel detectors was proven for cell sizes of  $50\text{ }\mu\text{m} \times 50\text{ }\mu\text{m}$  and column diameters of  $2.6\text{ }\mu\text{m}$ .  
135 The largest device had a number of 4000 cells and the efficiency of the column drilling process is above 99 %. The first prototypes of small cell 3D diamond pixel detectors read out more charge than any planar pCVD diamond detector. The measured relative hit efficiency of the 3D pixel detectors reached 99.3 % compared to a planar silicon device.

140 It was found that irradiated pCVD diamond detectors work reliably and there is no signal variation greater than 2 % up to an incident particle flux of  $20\text{ MHz/cm}^2$ . This was shown for a range of irradiations up to a maximum fluence of  $8 \cdot 10^{15}\text{ n/cm}^2$ . The beam induced current of a pCVD diamond is proportional to the flux and the leakage current is of the  $\mathcal{O}(1\text{ nA})$ . It was also  
145 demonstrated that it is possible to correct a large rate dependence that occurs in a small fraction of diamonds and is most likely due to surface properties.

#### Acknowledgements

We want to thank Bert Harrop at the Physics Department of the Princeton University for bump bonding the devices. The research leading to these results  
150 received funding from the European Union’s Horizon 2020 research and innovation program under grant agreement No. 654168. This work was also partially supported by the Swiss National Science Foundation grant #20FL20\_154216, ETH grant 51 15-1, the Swiss Government Excellence Scholarship ESKAS No. 2015.0808, the Royal Society Grant UF120106, the UK Science and Technology  
155 Facilities Council Grant ST/P002846/1 and the U.S. Department of Energy through grant DE-SC0010061

## References

1. Contardo D, Klute M, Mans J, Silvestris L, Butler J. Technical Proposal for the Phase-II Upgrade of the CMS Detector. Tech. Rep. CERN-LHCC-2015-010. LHCC-P-008. CMS-TDR-15-02; Geneva; 2015. URL: <http://cds.cern.ch/record/2020886>.  
160
2. Kagan H, et al. (RD42). Development of Diamond Tracking Detectors for High Luminosity Experiments at the LHC, HL-LHC and Beyond. Tech. Rep. CERN-LHCC-2018-015. LHCC-SR-005; CERN; Geneva; 2018. URL: <https://cds.cern.ch/record/2320382>.  
165
3. de Boer W, et al. Radiation hardness of diamond and silicon sensors compared. *Physica Status Solidi Applied Research* 2007;204:3004–10. doi:10.1002/pssa.200776327. arXiv:0705.0171.
4. Pernegger H, et al. Charge-carrier properties in synthetic single-crystal diamond measured with the transient-current technique. *J Appl Phys* 170 2005;97(7):73704–1. URL: <https://cds.cern.ch/record/909063>.
5. Zhao S. Characterization of the electrical properties of polycrystalline diamond films. Ph.D. thesis; The Ohio State University; 1994. URL: <http://wwwlib.umi.com/dissertations/fullcit?p9421043>.
6. Edwards AJ, et al. Radiation monitoring with diamond sensors in BABAR. *IEEE Transactions on Nuclear Science* 2004;51(4):1808–11. doi:10.1109/TNS.2004.832634.  
175
7. Eusebi R, Wallny R, Tesarek R, Dong P, Sfyrla A, Trischuk W, Schrupp C. A Diamond-Based Beam Condition Monitor for the CDF Experiment. 2006:709 –12. doi:10.1109/NSSMIC.2006.355953.  
180
8. Schaefer D. The ATLAS Diamond Beam Monitor: luminosity Detector on the LHC. Tech. Rep. ATL-INDET-PROC-2015-009; CERN; Geneva; 2015. URL: <https://cds.cern.ch/record/2034225>.

9. Parker S, Kenney C, Segal J. 3D - A proposed new architecture for solid-state radiation detectors. *Nuclear Instruments and Methods in Physics Research Section A: Accelerators, Spectrometers, Detectors and Associated Equipment* 1997;395(3):328 –43. URL: <http://www.sciencedirect.com/science/article/pii/S0168900297006943>. doi:[https://doi.org/10.1016/S0168-9002\(97\)00694-3](https://doi.org/10.1016/S0168-9002(97)00694-3).
10. Oh A, et al. (RD42). A 3D diamond detector for particle tracking. *Nuclear Instruments and Methods in Physics Research Section A: Accelerators, Spectrometers, Detectors and Associated Equipment* 2015;786:97 – 104. URL: <http://www.sciencedirect.com/science/article/pii/S0168900215003496>. doi:<https://doi.org/10.1016/j.nima.2015.03.033>.
11. Pimenov SM, et al. Femtosecond laser microstructuring in the bulk of diamond. *Diamond and Related Materials* 2009;18(2):196 –9. URL: <http://www.sciencedirect.com/science/article/pii/S0925963508003981>. doi:<https://doi.org/10.1016/j.diamond.2008.07.014>.
12. Sun B, Salter PS, Booth MJ. High conductivity micro-wires in diamond following arbitrary paths. *Applied Physics Letters* 2014;105(23):231105. URL: <https://doi.org/10.1063/1.4902998>. doi:[10.1063/1.4902998](https://doi.org/10.1063/1.4902998). arXiv:<https://doi.org/10.1063/1.4902998>.
13. Kornmayer A, Müller T, Husemann U. Studies on the response behaviour of pixel detector prototypes at high collision rates for the CMS experiment. 2015. URL: <https://cds.cern.ch/record/2264667>; presented 04 Dec 2015.
14. Forcolin GT, Oh A, Da Via C. Development and simulation of 3D diamond detectors. 2018. URL: <https://cds.cern.ch/record/2636028>; presented 2018.
15. Garcia-Sciveres M, et al. The FE-I4 Pixel Readout Integrated Circuit.

- Tech. Rep. ATL-UPGRADE-PROC-2010-001; CERN; Geneva; 2010. URL: <https://cds.cern.ch/record/1231359>.
16. HIPA. High Intensity Proton Accelerator at PSI. <https://www.psi.ch/rf/hipa>; 2017.
17. piM1 beam line. Pion and electron fluxes in piM1. <http://aea.web.psi.ch/beam2lines/pim1c.html>; 2015.
18. Bachmair F. CVD Diamond Sensors In Detectors For High Energy Physics. Ph.D. thesis; Zurich, ETH; 2016. URL: <https://inspirehep.net/record/1503510/files/CERN-THESIS-2016-163.pdf>.
19. Snoj L, Žerovnik G, Trkov A. Computational analysis of irradiation facilities at the JSI TRIGA reactor. *Applied Radiation and Isotopes* 2012;70(3):483 –8. URL: <http://www.sciencedirect.com/science/article/pii/S0969804311005963>. doi:<https://doi.org/10.1016/j.apradiso.2011.11.042>.
20. Edwards AJ, et al. Radiation monitoring with diamond sensors in BABAR. In: *2003 IEEE Nuclear Science Symposium. Conference Record (IEEE Cat. No.03CH37515)*; vol. 1. 2003:83–86 Vol.1. doi:[10.1109/NSSMIC.2003.1352003](https://doi.org/10.1109/NSSMIC.2003.1352003).